Joule

CellPress
REVIEWS

Review

Li-free Cathode Materials for High Energy Density Lithium Batteries

Liping Wang,[1,2] Zhenrui Wu,[1] Jian Zou,[1] Peng Gao,[3] Xiaobin Niu,[1] Hong Li,[2,4,5,*] and Liquan Chen[2,4,5]

Conversion-type cathode materials, such as transition metal halides, chalcogenides, and oxides, demonstrate high operational voltages and high specific capacities, offering high energy densities for rechargeable lithium-metal batteries. In this review, a series of low-cost, environmentally benign, and high energy density Li-free cathode materials are selected based on thermodynamic calculations. Coupled with Li/C anodes, these cathodes (e.g., S, FeF_3, CuF_2, FeS_2, and MnO_2) have the potential to offer energy densities of 1,000–1,600 Wh kg^{-1} and 1,500–2,200 Wh L^{-1} at the cell level. Their main challenges, including capacity fading, high voltage hysteresis, large volume change, and parasitic reactions with electrolytes, are discussed. Strategies to circumvent these issues based on the state-of-the-art technologies are summarized. It seems that all of these challenges are able to be solved. We believe that with the development of practical Li-metal-based anodes and solid-state electrolytes, conversion-type cathodes have a promising future for the next-generation high energy density energy storage devices.

Introduction

The history of lithium (Li) batteries dates back to the 1950s when Li metal was used as the anode in non-aqueous primary cells, such as Li/$(CF)_n$,[1] Li/SO_2,[2] Li/FeS_2,[3] Li/MnO_2,[4] and $SOCl_2$.[5] Later, in the early 1970s, intensive efforts to develop Li-metal-based rechargeable batteries began, as it was found that Li^+ can intercalate and de-intercalate into layered dichalcogenides. Coin cells consisting of a Li-Al alloy anode, a TiS_2 cathode, and a $LiClO_4$-dioxolane electrolyte were successfully brought into market via Exxon in 1977–1979.[6] Meanwhile, a series of Li-free cathodes were investigated, e.g., TiS_2, MoS_2, VS_2, CrS_2, NbS_2, and TaS_2.[6,7] Unfortunately, these Li-metal-based rechargeable batteries suffer from explosion hazards as a result of Li dendrites piercing the separator.[8] Several fire incidents resulted in decreased interest in the development of Li-metal batteries accompanied with a well-known battery recall by the Moli Energy company in 1989.[9]

Figure 1 shows the timeline for the development of Li-metal batteries to Li-ion batteries (LIBs) from 1972 to 2019. Goodenough and co-workers explored the Li-containing cathodes $LiCoO_2$ in 1980[10] and $LiMn_2O_4$ in 1984,[11,12] which had an operational voltage of ~4.1 V versus Li^+/Li. Yazami and Touzain demonstrated that the layered structure of graphite had good Li intercalation behavior at ~0.2 V versus Li^+/Li.[13] As they are Li-containing cathodes, the Li-metal anode can be replaced by a Li-free one, such as carbon. In 1990, the first commercial Li-ion battery composed of a $LiCoO_2$ cathode, a petrol-coke carbon anode, and a $LiPF_6$-PC electrolyte was developed by Sony. This is a milestone in the history of rechargeable Li batteries. Afterward, a number of intercalation-type cathodes were reported, e.g., Li_2MnO_3 in 1993,[14,15] $LiFePO_4$ in 1997,[16] Li_2MO_3-$LiM'O_2$ in 1997,[17–19] and $Li(NiMnCo)_{1/3}O_2$ (denoted as NMC) in 2003.[20,21] On the other hand, nanosized

Context & Scale

Lithium-ion batteries (LIBs) have a superior energy density compared to other rechargeable batteries. However, commercial LIBs have challenges to exceed the target of 300 Wh kg^{-1}. Exploring energy storage devices with energy densities higher than 300 Wh kg^{-1} is highly desired for long-range electric vehicles, advanced portable electronic devices, and many other applications.

Because of the renaissance in the study of lithium-metal anodes and the rapid development of solid-state electrolytes, revisiting Li-free cathodes with high energy densities is necessary. Herein, we have screened several of the most promising cathode materials (e.g., S, FeF_3, CuF_2, FeS_2, and MnO_2) based on thermodynamic calculations. They have the potential to offer energy densities of 1,000–1,600 Wh kg^{-1} and 1,500–2,200 Wh L^{-1} at the cell level. Recent advances regarding their application in rechargeable lithium batteries are reviewed. Their intrinsic limitations, including low practical specific capacity, high voltage hysteresis, and short cycling life, are discussed, and the corresponding solutions are suggested. All of these challenges could be overcome. Therefore, low-cost Li-free cathode materials with a

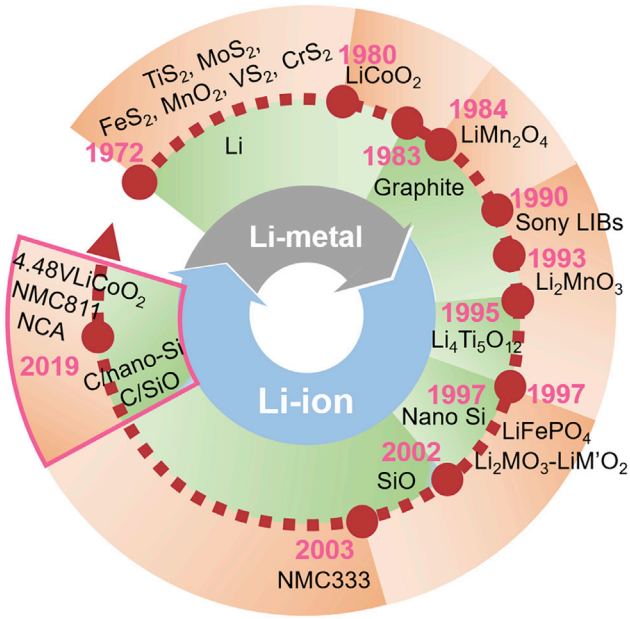

Figure 1. The Timeline for the Development of Lithium-Metal Batteries to Lithium-Ion Batteries from 1972 to 2019

Si,[22] $Li_4Ti_5O_{12}$,[23] and SiO[24] were developed as anode materials. All of these materials have been used in commercial batteries.

Energy density is a key parameter of batteries. It increased from ~35 Wh kg^{-1} for the TiS_2/Li system to 80 Wh kg^{-1} for the first $LiCoO_2$/C made in 1990. Thanks to the scientific and technical achievements over the last 30 years, the energy density of intercalation-type LIBs has gradually increased. Given that the nano-Si and graphite composite anode provides a specific capacity of 450 mAh g^{-1} and that the counterpart $LiNi_{0.8}Mn_{0.1}Co_{0.1}O_2$ cathode offers a practical specific capacity of 200 mAh g^{-1}, a typical pouch cell can provide an energy density of 300 Wh kg^{-1}. In order to extend driving range and decrease the cost, increasing the energy density above 300 Wh kg^{-1} is still highly desired by battery and electrical vehicle manufacturers.

Among many electrochemical energy storage systems, Li-metal-based batteries have high energy densities due to the light weight (6.941 g mol^{-1} and 0.534 g cm^{-3}) and low chemical potential (−3.04 V versus SHE) of Li. In addition, Li^+ has a smaller radius (0.76 Å) than other alkaline metal ions (Na^+ for 1.02 Å and K^+ for 1.38 Å) and has weaker interactions with lattice atoms than multivalent cations (Al^{3+}, Mg^{2+}, and Zn^{2+}), which guarantee a higher power rate and longer cycling life. Recently, a renaissance in the research on Li-metal anodes is aggressively progressing.[25–29] This is especially promoted by the development of solid-state electrolytes with a high ionic conductivity of 10^{-2} S cm^{-1} at room temperature.[30–33] The use of a solid-state electrolyte can restrain the growth of Li dendrites and prevent continued side reactions. Actually, the first electric vehicle (EV) powered by Li-metal polymer-based solid-state batteries, branded Bolloré Bluecar, was deployed by Autolib in 2011.[34] It had an energy density of ~100 Wh kg^{-1} at pack level at an operating temperature of 60°C–80°C.[35] This type of batteries can cycle over 1,000 times. Although the energy density of the battery is not outstanding and the batteries have to operate at an elevated temperature, the commercial application shows the feasibility of developing rechargeable Li batteries using a metallic Li anode. Since the anode

conversion reaction mechanism are competitive and promising components in rechargeable lithium batteries for next-generation high energy density devices.

[1]School of Materials and Energy, University of Electronic Science and Technology of China, Chengdu 611731, China

[2]Tianmu Lake Institute of Advanced Energy Storage Technologies, Changzhou 213300, China

[3]Electron Microscopy Laboratory, School of Physics, Peking University, Beijing 100871, China

[4]Institute of Physics, Chinese Academy of Sciences, Beijing 100190, China

[5]Center of Materials Science and Optoelectronics Engineering, University of Chinese Academy of Sciences, Beijing 100049, China

*Correspondence: hli@iphy.ac.cn

https://doi.org/10.1016/j.joule.2019.07.011

contains Li, it is unnecessary that both the cathode and the anode contain Li. The cathodes could be Li-free and the reversible Li storage mechanism can change from the intercalation reaction to the conversion reaction.[36–39] Looking back in history, it is interesting to find that the study of Li-related batteries could experience a "reincarnation," as demonstrated in Figure 1.

In consideration of their potential advantages, low cost, environmental benignity, easy synthesis, insensitivity to moisture, and high energy density, Li-free cathodes could become competitive candidates compared to Li-contained cathodes. In this review paper, we screen out the most promising high energy density conversion-type Li-free cathodes based on thermodynamic calculations and list their electrochemical performances reported in literature. Problems with regard to capacity fading, voltage hysteresis, volume change, and side reactions for Li-free cathodes are discussed and possible solutions are provided.

Energy Density Calculations for Li-free Cathodes

A typical conversion reaction can be expressed as

$$MX_m + nLi \leftrightarrow nLiX_{m/n} + M \text{ (M = transition metal; X=F, Cl, O, S, N, or P).} \quad \text{(Equation 1)}$$

Here, M represents reduced metal. In nearly all reports, the product is nanosized metal particles (< 5 nm[36,40–43]) distributed within the amorphous $LiX_{m/n}$ matrix. Its electromotive force (emf) (denoted as ξ) can be calculated based on the Nernst equation,

$$\Delta_r G = n\,\Delta G_f(LiX_{m/n}) - \Delta G_f(MX_m) = -n\,F\,\xi, \quad \text{(Equation 2)}$$

where $\Delta_r G$ is the difference in Gibbs free energy (kJ mol^{-1}) for the reaction, ΔG_f is the Gibbs free energy of formation (kJ mol^{-1}), F is Faraday's constant (96,485 C mol^{-1}), and n is the number of electron (mol) for this reaction. Standard thermodynamic data for the ΔG_f can be obtained via handbook[44] or by first principle calculations.[45]

Accordingly, the specific capacity Q (mAh g^{-1}) for MX_m cathode materials can be calculated from Equation 3:

$$Q = n\,F/3.6\,M, \quad \text{(Equation 3)}$$

where M is the molecular weight (unit g mol^{-1}, e.g., 112.84 g mol^{-1} for FeF_3).

Thus, based on Equations 2 and 3, the gravimetric energy density E_m (Wh kg^{-1}) can be obtained directly from Equation 2 or by multiplying the specific capacity Q (mAh g^{-1}) by emf (V).

$$Em = \xi \times Q. \quad \text{(Equation 4)}$$

Meanwhile, the volumetric energy density E_v (Wh L^{-1}) is obtained by the following equation:

$$Ev = Em * \rho, \quad \text{(Equation 5)}$$

where ρ is the theoretical density (g cm^{-3}, e.g., 2.01 for S, 3.52 for FeF_3, 5.02 for MnO_2, and 4.98 for FeS_2).

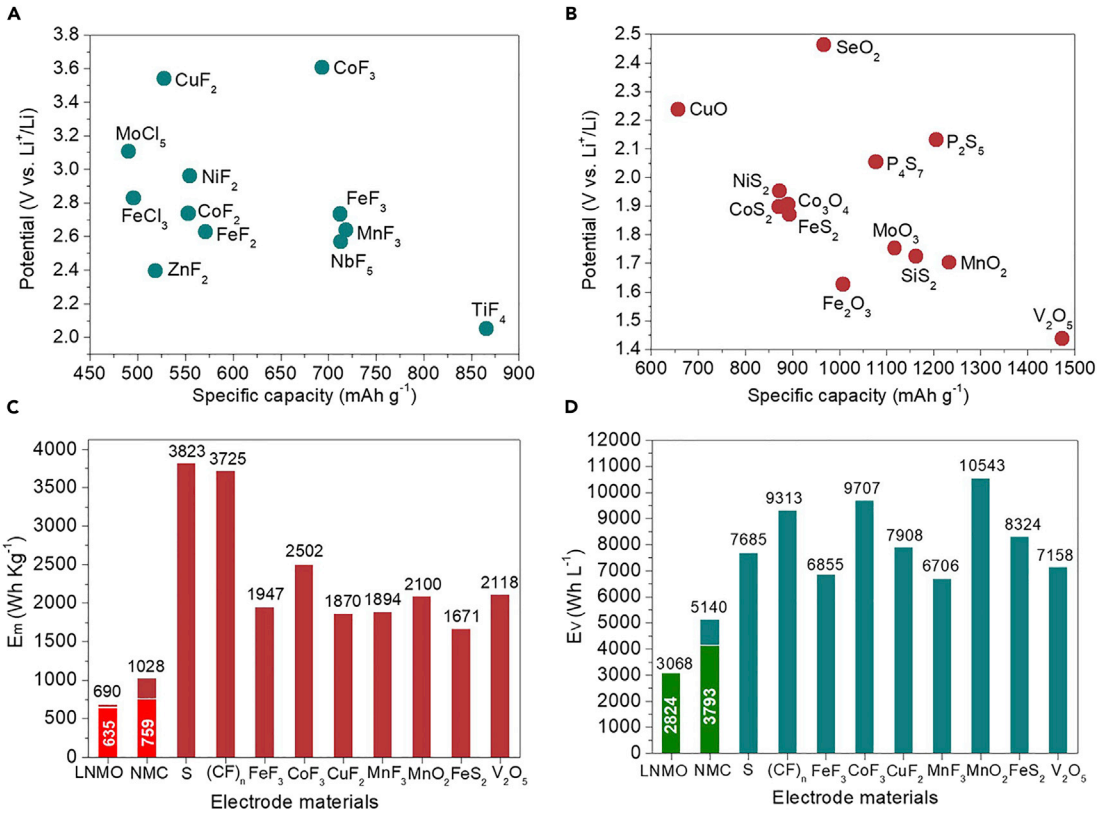

Figure 2. Low-Cost Li-free Cathodes with High Energy Density >1,200 Wh kg^{-1}

(A and B) Theoretical specific capacity and operational voltage for Li-free cathodes, halides (A), and chalcogenides and oxides (B).

(C and D) Some Li-free cathodes with (C) high gravimetric energy density and (D) high volumetric energy density. $LiNi_{0.5}Mn_{1.5}O_4$ (denoted as LNMO), $Li(NiMnCo)_{1/3}O_2$ (denoted as NMC), a primary cell cathode $(CF)_n$, and S are imported for comparison.

Based on Equations 1, 2, 3, 4, and 5, we screen a series of low-cost, nontoxic Li-free cathodes with high energy densities (>1,200 Wh kg^{-1} as inclusion criteria), as displayed in Figure 2. Metal phosphides and chromium oxides are excluded because of their toxicity. Figures 2A and 2B show their operational voltages and theoretical specific capacities. It is found that, in Figure 2A, metal fluorides have the highest emf value because F elemental has the highest electronegativity (χ_s = 4.19, 3.61, 2.87, and 2.59 for F, O, Cl, and S, respectively). Figure 2B reveals that multi-electron reactions, such as chalcogenides and oxides, provide high specific capacity (650–1,500 mAh g^{-1}) with mediocre operational voltages (1.4–2.5 V). Li-free cathodes show the highest gravimetric and volumetric energy densities (Figures 2C and 2D). For a clear view, we list the most common Li-ion battery cathodes: NMC, $LiNi_{0.5}Mn_{1.5}O_4$ (denoted as LNMO), $(CF)_n$, and S. The practical energy densities for NMC and LNMO are marked in the corresponding columns. Transition metal fluorides MF_x (M = Fe, Co, Cu, or Mn), MnO_2, and FeS_2 demonstrate their superiority with energy densities >1,600 Wh kg^{-1} and >6,700 Wh L^{-1}.

Predicting the Energy Density of Rechargeable Li Batteries

Here, we take the Co- and Li-free cathode FeS_2 as an example to estimate its energy density at the cell level, as shown in Figure 3. The thicknesses of Al and Cu are 6 and 5 μm, respectively (half of the real value of 12 and 10 μm due to the double-sided pasting design). The electrolyte has a thickness of 30 μm. The cathode is fixed at 100 μm with a porosity of 25%. The anode is a Li (85 wt %)/C (15 wt %) composite

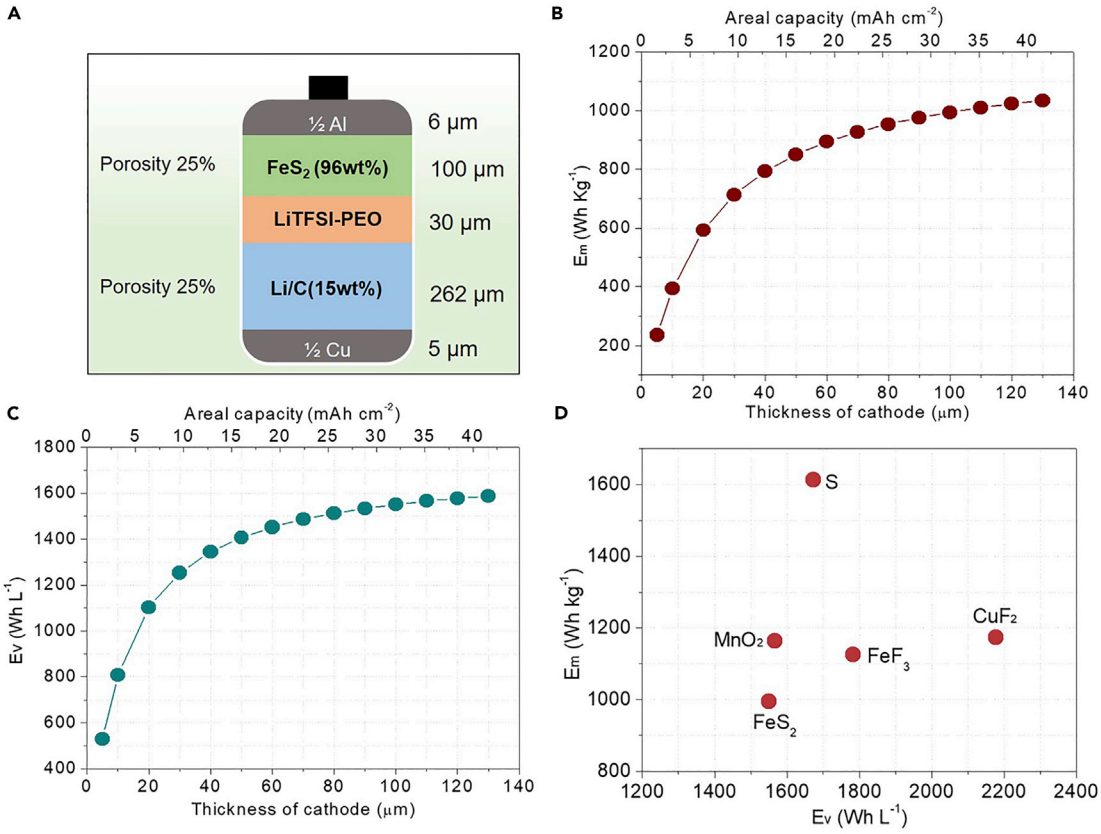

Figure 3. A Prediction of Energy Density for Solid-State Li-Metal Batteries

(A) A schematic of the FeS_2-cathode-based solid-state battery.

(B and C) The gravimetric energy density (B) and volumetric energy density (C) at the cell level as a function of FeS_2 cathode thickness and areal capacity.

(D) The energy density for solid-state Li-metal batteries using the most promising Li-free cathodes: S, FeF_3, CuF_2, MnO_2, and S.

with a porosity of 25%. The N/P ratio is 1.2. The emf value for FeS_2 is 1.87 V, which is lower than the oxidation voltage of the PEO-polymer-based electrolyte, and thus we apply LiTFSI-PEO with a density of ~1.3 g cm^{-3} as the electrolyte. Given the 3 wt % binder and 1 wt % carbon additives in the cathodes and 2 wt % casing and tab in the whole cell, the cell energy densities as a function of cathode thickness or areal capacity are presented in Figures 3B and 3C. An areal capacity of 4 mAh cm^{-2} results in a cell with a 455 Wh kg^{-1} energy density. The 100-μm-thick FeS_2 cathode provides a cell energy density of 995 Wh kg^{-1} (1,550 Wh L^{-1}) and an areal capacity of 32 mAh cm^{-2}. This solid-state Li/PEO-LiTFSI/FeS_2 cell has a similar volumetric energy density but a much higher gravimetric energy density than the same cell using liquid electrolyte, as indicated in Figure S1.

Based on the same parameters shown in Figure 3A, the cell energy densities are calculated to be 1,172 Wh kg^{-1} (2,178 Wh L^{-1}) for CuF_2, 1,125 Wh kg^{-1} (1,782 Wh L^{-1}) for FeF_3, 1,163 Wh kg^{-1} (1,566 Wh L^{-1}) for MnO_2, and 1,613 Wh kg^{-1} (1,673 Wh L^{-1}) for S (Figure 3D). It should be noted that Li-containing anodes with a higher percentage of carbon, a higher N/P ratio, and cathodes mixed with solid-state electrolytes, could be necessary strategies for controlling the volume change and achieving better electrochemical performances. Consequently, the gravimetric and volumetric energy densities will decrease. It still remains much higher than ~300 Wh kg^{-1} of current Li-ion batteries.

Table 1. Reported Capacity and Operational Voltage for Li-free Cathodes

Materials	σ_e (S cm^{-1})	1st Q_{dis} (mAh g^{-1})	1st Potential (V versus Li$^+$/Li)	2nd Q_{dis} (mAh g^{-1})	Potential Window	Capacity Retention (mAh g^{-1})
S	5 × 10^{-30}[48]	800 (0.1C)	2.1	810	1.7–3.0 V	750 (100th)[49]
$(CF)_n$	10^{-12}–10^{-14}[50]	896(1C)	1.95	0	1.5–3.0 V	0[51]
FeF_3	10^{-17}[52]	550 (100 mA g^{-1})	1–4	550	1.0–4.0 V	520 (400th)[53]
CoF_3	none	1011 (5 mA g^{-1})	1.5	420	0–4.0 V	400 (14th)[54]
CuF_2	none	530 (5 mA g^{-1})	3.25	172	1.5–4.5 V	58 (3rd)[40]
FeS_2	10^{-6}–1[55]	907 (1C)	1.6	820	1.0–3.0 V	720 (100th)[56]
MnO_2	0.02[57]	780 (500 mAg^{-1})	0.4	720	0–3.0 V	847 (250th)[58]

Practical Electrochemical Performances

The electrochemical performances and the discharge-charge voltage profiles of four Li-free cathodes (S, FeF_3, CuF_2, and MnO_2) in liquid electrolyte systems are summarized in Table 1 and Figure 4. It can be seen that the reported performances are far from the theoretical predication. Their initial discharge specific capacities are closed to the theoretical values, while their operational voltages are lower than their emf values. They suffer from fast capacity decays after the 2nd cycle. Their rate performances are not good. In addition, the voltage hysteresis is significant, which is regarded to be related to low electronic conductivities, low diffusion coefficients of Li ions (10^{-17}–10^{-19} cm^2 s^{-1}), and sluggish phase transformation kinetics.[46,47] In summary, their poor performances need to be further investigated in four aspects: real reaction pathways, voltage hysteresis, volume change, and side reactions. These will be discussed below.

Real Reaction Pathways

The emf value is calculated based on the bulk phase. In the practical case, there are deviations as the lithiation process normally generates nanocrystalline or amorphous phases. The formation energy in an amorphous structure is different from that of a crystalline phase.[60–62] Seo et al. found that nanosized metal particles (<2 nm, M = Cu, Fe, and Ni) with high surface energy in transition metal fluorides show an emf value of 0.19–1.02 V lower than those of the bulk particles.[63]

For a one-step phase transition (as shown in Equation 1), the emf value is constant during the whole reaction. While the practical reaction mechanism is complex, the Li storage could occur in several stages. Here, we take FeF_3 as an example, it shows three voltage stages of FeF_3 from open circuit voltage (OCV) to 0.2 V (Figure 5).[46,61]

Stage I: $FeF_3+Li^++e^-\rightarrow LiFeF_3$, at ~3.3 V versus Li$^+$/Li, which is an intercalation reaction.
Stage II: $LiFeF_3+2Li^++2e^-\rightarrow Fe+3LiF$, at ~1.9 V, which is a conversion reaction.
Stage III: Fe+LiF+xLi^++xe^-àFe/xLi/LiF, below 0.5 V, where Li accumulates at the interface between nanosized Fe and amorphous LiF. In real applications, the capacity at low voltage is not available for cathodes.

Similar electrochemical transformations occur in TiS_2, MoS_2, and FeS_2 cathodes.[64,65] For FeF_2, Karki et al. discovered a topotactic reaction mechanism with a checkboard-like nanodomain in the lithiated FeF_2.[66] For FeOF, LiF, metallic Fe, and a cubic

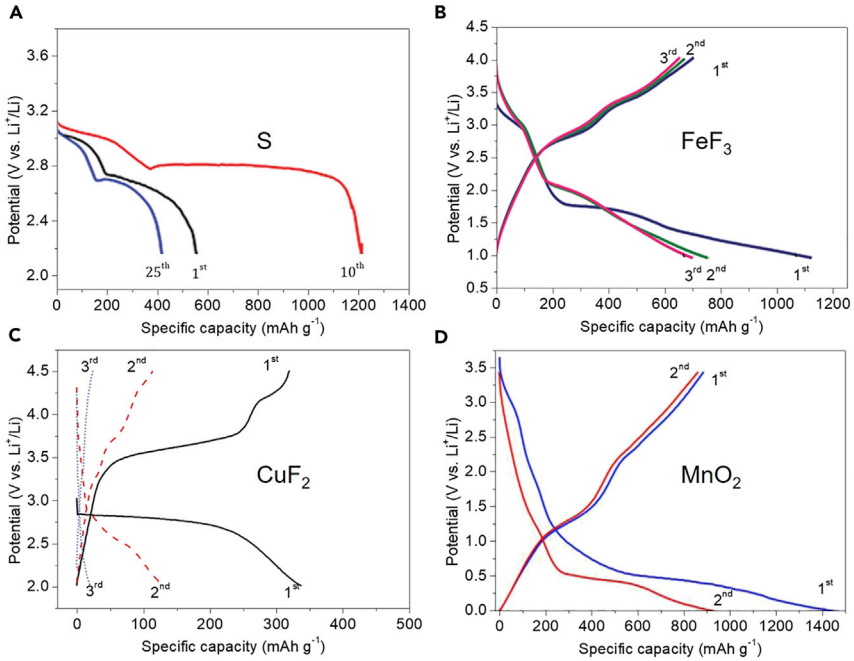

Figure 4. Typical Discharge-Charge Profiles of Li-free Cathodes

Cycling performance of (A) S (reproduced from Lv et al.[49]), (B) FeF_3 (reproduced from Fu et al.[53]), (C) CuF_2 (reproduced from Krahl et al.[59]), and (D) MnO_2 (reproduced from Zang et al.[58]).

rocksalt phase Li-Fe-O-F are formed instead of Li_2O.[67] Above the emf value of 1.7 V, MnO_2 undergoes the intercalation reaction to form $LixMnO_2$ ($0 < x < 1$).[68]

Large Voltage Hysteresis

Conversion reaction-type materials suffer from a severe overpotential η. η is a voltage deviation between the thermodynamic potential and the experimental value. Far from the emf of 2.73 V, the actual conversion reaction upon FeF_3 occurs at 1.89 V,[46] as shown in Figure 5. It is known that the η includes ohmic polarization, reaction rate polarization, and concentration polarization. Ohmic loss is related to the internal resistance and is normally at the mΩ level in commercial cells thanks to multiple-layer cell design. The reaction rate overpotential is related to the charge exchange rate. Concentration overpotential is always the rate-determining step as a result of sluggish Li^+ transport in the solid state and across the interface. Ohmic polarization and reaction rate polarization should be zero during relaxation, as shown in titration measurements of using the potentiostatic intermittent titration technique (PITT) and the galvanostatic intermittent titration technique (GITT). Concentration polarization may not be mitigated completely even after a long relaxation period.[69] Such phenomenon has been called zero-current overpotential. Doe et al. explained that polarizations originate from the presence of different reaction paths through the phase diagram under nonequilibrium states.[45] For a conversion-type reaction at room temperature, voltage hysteresis is related to both thermodynamics (asymmetrical reaction pathway) and sluggish kinetics (transport of host atoms). For example, the overpotential of α-Fe_2O_3 in the first cycle is much higher than the following cycles, as its electronic conductivity increases from 10^{-8} to 25 S cm^{-1} in the discharged state with the formation of nanostructure, then decreases to ~10^{-2} S cm^{-1} in the oxidized state.[70] Wang et al. reported that the formation of Fe is crucial for mitigating the voltage hysteresis of FeF_3 due to the formation of a good electron transport pathway in the insulating LiF matrix.[71] Note that RuO_2 also presents high

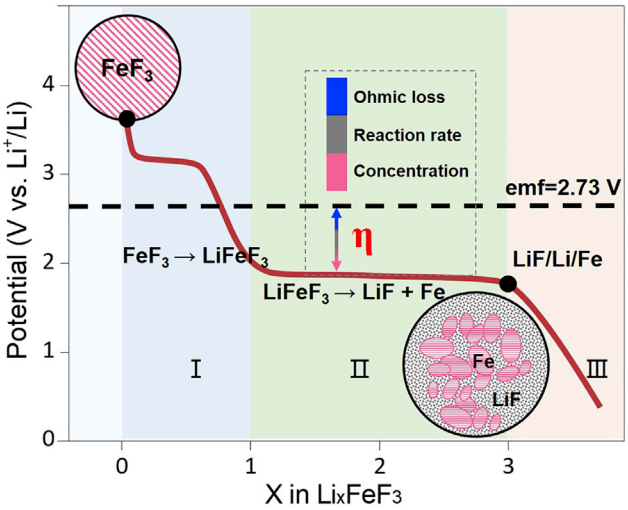

Figure 5. The Phase Reactions and Hysteresis of the FeF_3 Cathode in Lithium Batteries

voltage hysteresis even though it is a metallic conductor.[72] The main origin is related to the sluggish diffusion of host atoms during phase transformation instead of the transport of electrons and ions.

Large Volume Change

The shuttle of Li^+ or Li^+-solvents between the cathode and anode normally causes lattice expansion or contraction. Typically, the volume decreases by 6.12% from LNMO to $Ni_{0.5}Mn_{1.5}O_4$[73] and swells by 1.09% from $Li(NiCoMn)_{1/3}O_2$ to $(NiCoMn)_{1/3}O_2$[74] and 10.7% from graphite to LiC_6.[75] Here, we calculate the volume change, considering both the cathode part (Figure 6A) and the active materials (assume a sum of the cathode and the Li anode, Figure 6B) at a 100% depth of discharge (DOD) based on the theoretical density. The S to Li_2S has a volume increase of 78.69% and the $(CF)_n$ to LiF and C has a volume expansion of 22.06%. FeF_3, CoF_3, and CuF_2 have a comparatively smaller volume expansion of 14.06%, 19.69%, and 11.54%, respectively. For the four-electron-driven reaction, FeS_2 and MnO_2 have a huge volume expansion of 159.20% and 115.43%, respectively, to accommodate Li. In contrast, all of the active materials in the whole cell (e.g., from FeF_3-Li to LiF-Fe) give rise to a volume contraction at 100% DOD. The Li-FeS_2 couple demonstrates the smallest volume contraction, 17.93% versus 33.28% in Li-S, 40.40% in Li-$(CF)_n$, 48.54% in Li-FeF_3, 48.08% in Li-CoF_3, 46.45% in Li-CuF_2, and 46.17% in Li-MnO_2. Figure 6C presents the detailed volume expansion in FeS_2 cathodes and the volume contraction in the cell at 100% DOD, which is calculated based on 1 mol per reaction. The cell contraction (ΔV −17.93%) is mainly due to the consumption of the Li-metal anode.

In other words, Li-metal batteries have significant volume changes in principle. The volume change at the electrode level is more significant than that at the cell level. Active materials, which undergo a huge expansion or shrinkage, could pulverize and crack during cycling. This will lead to irreversible structural damage and loss of electrical contact with the binders and the current collector. In addition, exposing a fresh surface continuously brings in a rapid capacity decay. In the real cell, a flooded electrolyte is needed to accommodate the volume change, which leads to the decrease in energy density.[76] In order to achieve a good cycling performance, volume control changes within 10% for the cell and 20% for the electrode material

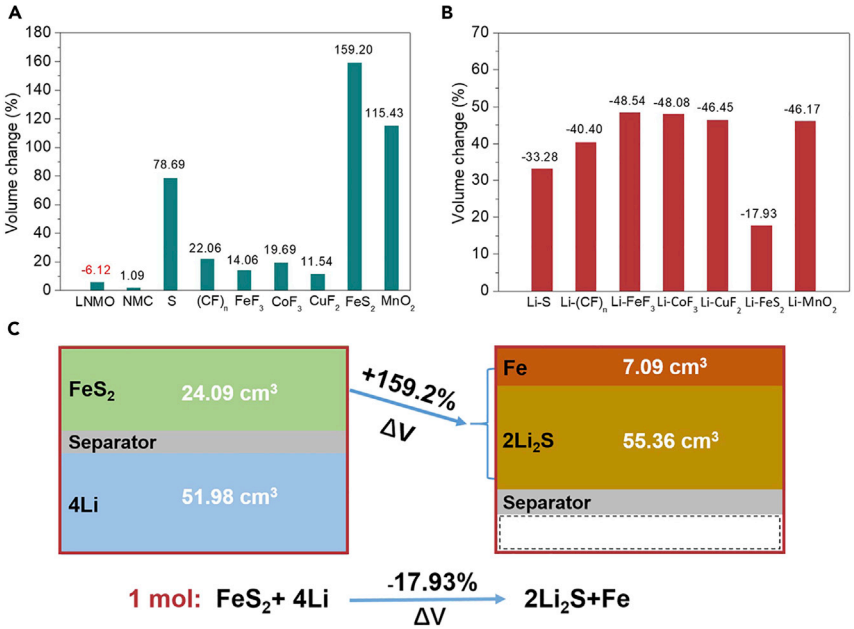

Figure 6. Volume Changes of the Cathode Materials and the Active Materials in Cells

(A) Theoretical volume changes for the Li-free cathode materials at 100% DOD.

(B) Theoretical volume changes for the active materials including the cathode and the Li-metal anode at 100% DOD. LNMO and NMC at 100% DOC are imported for comparison.

(C) The volume changes for FeS_2 cathodes and active materials in the cell per mol reaction.

are suggested. Therefore, rechargeable Li batteries using Li-free cathodes rely heavily on cell and electrode designs. It is noteworthy that this type of cell initially shrinks after assembling, which is much easier to handle than the expansion scenario for practical applications.

Side Reactions

A typical commercial battery needs to have a Coulombic efficiency over 99.98% for good cyclability.[77] Parasitic reactions in the battery, including chemical and electrochemical reactions, are detrimental to cycling life because they normally consume the active Li and produce undesirable species. Assisted by the surface reactions, the instability in the phase structure also evolves from the surface to the core at an atomic level. The Li-free cathodes mentioned above are transformed into nanosized grains (<5 nm) after the discharge process. Nanosized metals can be easily dissolved into the carbonate-based electrolyte and migrate into the anode side.[40] Meanwhile, the nanosized transition metal particles have empty 3d orbitals and a high surface area, giving rise to highly catalytic activity that promotes the cathode-electrolyte interface (CEI) formation. Cathodes that undergo a large volume change during discharge-charge will expose a bare surface continuously and promote undesirable side reactions. Meanwhile, the stability of the anions should also be paid. Take CuF_2 as an example: it is reported as a cathode in a fluoride-ion battery taking advantage of the high ionic conductivity of fluorid.[78] In this way, F^- may travel and reside in new sites under an electrical field. The other anion S^{2-} in addition with polysulfides (S_8^{2-}, S_6^{2-}, S_4^{2-}, etc.) can shuttle to the anode sides and lose its electrochemical activity.[79] Note that the chemical stability under the ambient conditions should also be considered, as it is associated with transportation and storage costs. It is known that the S^{n-} in chalcogenides is prone to be S^0 in air or to form H_2S in moisture,[8] and metal fluorides can be

oxidized in air at elevated temperatures, such as FeF_2 to FeOF in temperatures of 150°C–300°C.[80]

Strategies to Improve Their Electrochemical Performances

To achieve better electrochemical performances in terms of specific capacity, cycling life, and rate capability, a number of strategies have been performed as below.

Nanostructure with a Conductive Matrix

Two main methods are used to improve the electrochemical performance of electrode materials with low electronic and ionic conductivities: reducing their sizes to the nanoscale and homogeneous mixing with a highly conductive matrix. A carbon-coated nanosized $LiFePO_4$ cathode is one successful example. We know that the Li^+ diffusion time t in solids is proportional to the square of the diffusion length L based on Equation 6,[81]

$$t = L^2/2D, \qquad \text{(Equation 6)}$$

where D is the Li^+ diffusion coefficient.

A decrease in the particle size apparently shortens the diffusion time, resulting in a fast Li^+ concentration equilibrium, which means a low polarization. Meanwhile, the nanosize material with high surface area brings about a high contact area with the electrolyte; thus, it is surrounded with a high Li^+ flux. Moreover, nanostructured materials have more tolerance to stress and strain from local changes in volume change.[82] For example, microsized CuF_2 has a specific capacity of 100 versus 250 mAh g^{-1} for the analogous nanosized material.[83] As for FeF_3, a smaller crystal size controlled by the milling time leads to a higher specific capacity.[84]

A conductive matrix with an electron transportation network around the active materials can effectively improve the kinetic behaviors and maintain good electronic contact. Moreover, an adhesion or coating on the active material surface effectively suppresses the dissolution and side reactions. Carbon materials are ideal coating materials because they are highly conductive and easily synthesized with controllable morphology and porosity.[85] For instance, the electrochemical performances of FeF_2-filled hollow carbon is superior to those of ball-milled carbon mixtures.[86] As for nano fibers of C/FeF_3, it gives a specific capacity of more than 500 mAh g^{-1} with almost no decay after 400 cycles.[53] For nanosized FeS_2 encapsulated with carbon, it delivers a specific capacity of 500 versus 300 mAh g^{-1} for the pristine.[87]

It should be noted that carbon coating is not feasible for all conversion-type materials because of the instability of the host materials at high temperature under reducing atmosphere. Therefore, other conductive materials, e.g., polyacrylonitrile (PAN),[88] polypyrrole (PPY),[89] and poly(3, 4-ethylenedioxythiophene) (PEDOT),[90] have been considered to enhance the capacity and cycling stability. The introduction of nanostructures and conductive matrices slightly diminishes the energy density in practical cells. Therefore, a well-built 3D electron pathway and a minimum weight and volume ratio are desirable. Carbon nanotubes, especially single-walled carbon nanotubes (SWCNTs), have been confirmed to be a favorable conductive additive for nanosized Si-based anodes to achieve good cycling performance.

Cation and/or Anion Doping to Tune the Electronic Structure

Metal fluorides have large band gaps and low electronic conductivities. A proper amount of substitution of F with O and S elements can improve the conductivity.

Concomitantly, it increases the capacity. Take $FeO_{0.67}F_{1.33}$ for example: it has a smaller voltage hysteresis (~0.7 V) than both FeF_3 and FeF_2 (~1.3 V) under a current rate of C/1,000.[46] As for FeOF, it has a theoretical specific capacity of 885 mAh g^{-1}, higher than the 571 mAh g^{-1} of FeF_2 and 712 mAh g^{-1} of FeF_3. Cationic substitution to form solid solution metal fluoride $M^1_xM^2_{1-x}F_y$ (M_1, M_2 are transition metals) is another effective strategy to improve the energy density and cycling life. Wang et al. prepared $Cu_{0.5}Fe_{0.5}F_2$ via a facile mechanochemical synthesis, which demonstrates an energy density higher than 1,000 Wh kg^{-1} and a good capacity retention behavior.[91] Recently, Fan et al. made full use of a $Fe_{0.9}Co_{0.1}OF$ cathode, reporting a high energy density of ~1,000 Wh kg^{-1} even after 1,000 cycles.[92]

Phase Control: Amorphous and Polymorphic

Amorphous structures with long-range disorder and isotropic properties exhibit features that are distinct from crystalline structures.[93] pulsed laser deposition,[94] reactive sputtering,[95] solvent exfoliation,[96] direct precipitation,[97] and electrochemical deposition[98] are several ways to obtain the amorphous phase. Because of excess surface energy and free enthalpy, amorphous materials have a smaller ΔG_f than crystalline materials. The emf is 2.72 V for amorphous and 2.14 V for crystalline (60 nm) RuO_2.[99] Because of the lack of well-defined ionic transportation channels and defects, amorphous materials show better kinetics than their crystalline counterparts. For instance, amorphous $FePO_4$ is more electrochemically active (140 mAh g^{-1}) than its trigonal phase (70 mAh g^{-1}).[100] Both amorphous FeOF and NiF_2 present high specific capacities above 500 mAh g^{-1}.[101,102]

Some of these Li-free cathodes have polymorphs. It is known that MnO_2 has a number of polymorphs, α-, β-, γ-, λ-, and δ-MnO_2.[103] FeS_2 has a pyrite phase and a marcasite phase. Polymorphs have different ΔG_f and band structures, resulting in different emf values and kinetics.[104] Jiao et al. designed a mesoporous nanosized β-MnO_2 with a specific capacity of 284 mAh g^{-1} in the 2.0–4.5 V range.[105] Control of the synthetic conditions, such as precursors, calcination temperature, and pressure, are usually performed to obtain the desired crystal phase. As claimed before, because the conversion reaction leads to the structure's destruction, the initial crystal structure impacts the microstructure of the products after several cycles less.

Increasing the Operational Temperature

The kinetic limitation of the Li-free cathodes can be significantly mitigated by increasing the operational temperature. Most of their conductivity (σ) values follow the Arrhenius equation,

$$\sigma = \sigma_o \exp(-E_a/RT) \text{or } \ln \sigma = \ln \sigma_o - \frac{E_a}{RT}, \qquad \text{(Equation 7)}$$

where σ consists of σ_e and σ_i (S m^{-1}), E_a is the activation energy (J mol^{-1}), R is the gas constant (8.314 J mol^{-1} K^{-1}), and T is the absolute temperature (K).

Increasing the temperature leads to the increase of conductivities and reaction kinetics, which results in the increase of specific capacity and rate performance. For example, the electronic conductivity of FeS_2 increases from 10^{-1} S cm^{-1} at 25°C to 100 S cm^{-1} at 400°C.[106,107] FeF_3 embedded in carbon black delivers a reversible specific capacity of 600 mAh g^{-1} at 70°C versus 367 mAh g^{-1} at 22°C.[106,108] It is worth noting that a high operational temperature (>60°C) enables a low Li-metal anode modulus, consequently, dendrite formation can be suppressed. However, the thermal stability of most liquid electrolytes is poor at elevated temperatures. In this case, batteries that use a solid-state electrolyte with a high thermal stability

should be favorable for operation at elevated temperature. Meanwhile, a cell operating at 60°C–80°C needs an extra heating system to maintain the temperature, which brings down the actual energy density of the system. Apparently, available energy density of the battery fades continuously during storage.

Surface Modifications

Li-free cathodes have a huge volume change and severe surface reactions with the electrolyte during the discharge-charge process. Surface modifications, including coating to optimize CEI, are necessary. On the one hand, surface coating prevents direct physical contact between the electrode and electrolyte. This is effective to suppress metal dissolution. On the other hand, surface coatings act as scaffolds to alleviate strain and prevent mechanical failure in the active materials. Moreover, reasonable coating species or additives can modify the CEI compositions, leading to a homogeneous, stable, and high ionic conductivity CEI. It is reported that a NiO coating on CuF_2 effectively suppresses Cu metal dissolution.[63] The use of lithium bis(fluorosulfonyl)imide (LiFSI) salt and the electrolyte additive lithium bis(oxalato)borate (LiBOB) modify the CEI composition and enhance the electrochemical properties.[109,110] Obviously, elastic CEI should be favorable for conversion-type cathodes. This needs further investigation.

Solid-State Electrolytes

Using a solid-state electrolyte to replace the conventional carbonate-based liquid electrolytes is helpful to suppress the metal dissolution and improve cyclic performance. As an example, FeS_2 can survive after 500 cycles in a PEO-based electrolyte.[111] In a solid-state electrolyte Li_2S-P_2S_5 system, FeS_2 delivers a specific capacity of ~700 mAh g^{-1} at 30°C and more than 800 mAh g^{-1} at 60°C with decent capacity retention ability (Figure 7).[64] The application of a solid-state electrolyte is effective in preventing the dissolution of nanosized Fe metal and LiS_x. The use of a solid electrolyte can permit the operation at an elevated temperature without significant performance decay and serious concern on safety. A higher operational temperature leads to an increase in ionic conductivity from 9.17×10^{-4} S cm^{-1} at 30°C to 4.4×10^{-3} S cm^{-1} at 60°C in the solid-state electrolyte Li_2S-P_2S_5 system, which can also mitigate electrochemical polarization.

Other Tactics Such As Voltage Control and Functional Binders

As the volume change is related to the amount of Li insertion, capacity control, or voltage window, control is a trade-off between capacity and cyclability. MnO_2 is used in the primary cell through a four-electron conversion reaction and is reversibly cycled in the voltage window of 1.5–4.0 V to form Li_xMnO_2 ($0 < x < 1$).[112] TiS_2 demonstrates a better cycling performance in the 1.5–3.0 V range than in the 1.0–3.0 V range.[113]

Functional binders with strong bonding effect, good flexibility, and mechanical integrity are always very important in improving their electrochemical properties. However, very few studies have been conducted to optimize the binder for conversion-type cathodes. Great efforts have been made toward developing suitable binders for nano-Si anodes, which occur with 300% local volume variation.[114,115] It is believed that the experiences of the nano-Si anode can be grafted into the development of effective binders for high capacity conversion-type cathodes.

Here, we make a schematic illustration to summarize the challenges and corresponding strategies in Li-free cathodes (Figure 8). All of these solutions could be used simultaneously to enhance their electrochemical performances. The introduction of nanostructure, conductive matrix, surface modification, high effective binder, and operation at

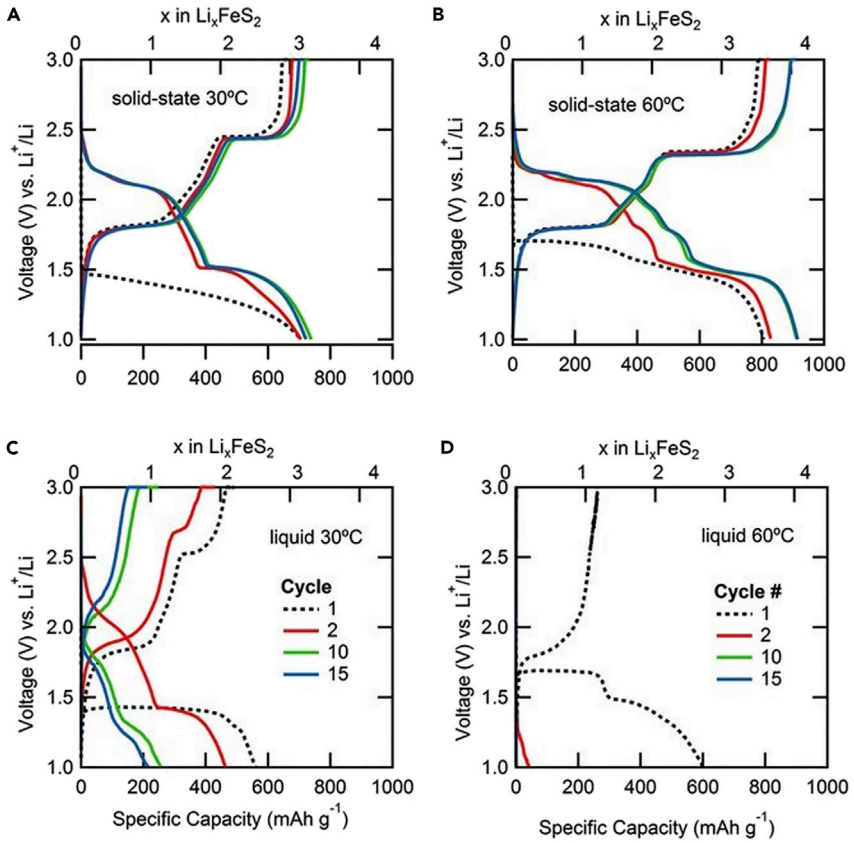

Figure 7. Electrochemical Performance of FeS_2 Cycled in a Solid-State Electrolyte Coin Cell and in a Liquid Coin Cell at 30°C and 60°C

The loading for the active material FeS_2 is approximately 1.6 mg, and the current rate is C/10 from the 2nd cycle. Reprinted with permission from Yersak et al.[64]

elevated temperatures are recommended for a balanced cell design. The solid-state electrolytes in place of liquid electrolytes typically leads to an increasing contact resistance with cycling due to the volume change and solid-solid interface. *In situ* growth of the solid-state electrolyte could be an effective way to keep good physical and chemical contact during cycling,[116] which has not been explored in conversion reaction-type cathodes yet. Strategies that are used in commercialized nano-Si anodes are good references for Li-free cathodes because they share the same issues with low electronic conductivity and large volume evolution.

Conclusions and Perspectives

In this review, we have screened a series of Li-free cathodes with high energy densities. Metal fluorides, sulfides, and oxides that undergo conversion reactions are attractive. The detailed reaction mechanisms for these materials are complex and heavily related to particle size, electrolyte composition, cut-off voltage, current rate, operational temperature, etc. Comprehensive and quantitative characterizations in real time and at the atomic level resolution are required for clarification.

For practical application, the main disadvantages, including voltage hysteresis, large volume change, and side reactions should be considered. Available strategies for cathode modifications are discussed, such as nanostructures embedded in the conductive matrix, elemental doping, surface modification, voltage control, phase

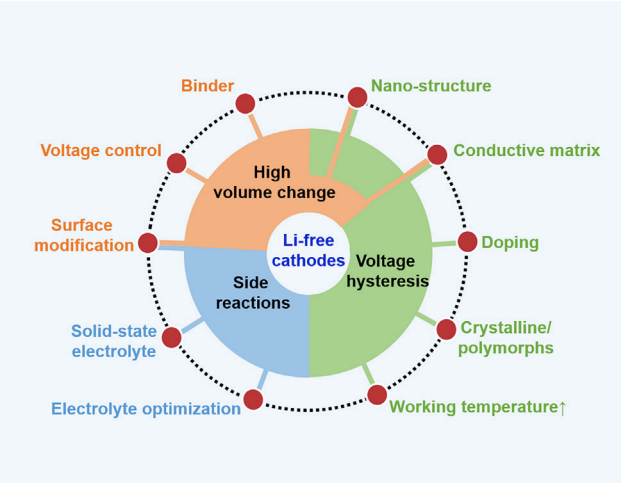

Figure 8. A Summary of the Challenges and Corresponding Strategies for Optimizing Li-free Cathodes

control, effective binders, and electrolyte additives, as well as *in situ* solidification. Combined solutions with synergistic functions could be effective to overcome all challenges. Li-free cathode will couple with Li-contained anode. Li-contained anode is recommended to couple with solid-state electrolyte to increase the safety and avoid the side reactions between Li and liquid electrolyte. With above possible solutions, we believe that Li-free cathodes are promising. We hope that this review could help attract attention for developing low-cost and high energy density rechargeable Li batteries using Li-free cathodes, which were explored as primary batteries many years ago.

SUPPLEMENTAL INFORMATION

Supplemental Information can be found online at https://doi.org/10.1016/j.joule.2019.07.011.

ACKNOWLEDGMENTS

This work is supported by the National Natural Science Foundation of China (51502032 and Y5JC011E21), National Key R&D Program of China (grant no. 2016YFB0100100), Beijing Municipal Science & Technique Commission (grant no. D181100004518003), and the Fundamental Research Funds for the Central Universities, China (no. ZYGX2016J044).

AUTHOR CONTRIBUTIONS

H.L. conceived and supervised the project. L.W., Z.W., J.Z., and H.L. wrote the manuscript. All the authors participated in the discussion.

REFERENCES

1. Watanabe, N. (1980). Two types of graphite fluorides $(CF)_n$ and $(C_2F)_n$, and discharge characteristics and mechanisms of electrodes of $(CF)_n$ and $(C_2F)_n$ in lithium batteries. Solid State Ionics *1*, 87–110.

2. Maricle, D.L., and Mohns, J.P. (1971). Electrochemical cell containing sulfur dioxide as the cathode depolarizer, US Patent 3567515.

3. Feuillade, G., and Perche, P. (1975). Ion-conductive macromolecular gels and membranes for solid lithium cells. J. Appl. Electrochem. *5*, 63–69.

4. Dampier, F.W. (1974). The cathodic behavior of CuS, MoO_3, and MnO_2 in lithium cells. J. Electrochem. Soc. *121*, 656–660.

5. Dey, A.N. (1976). Experimental optimization of Li/$SOCl_2$ primary cells with respect to the electrolyte and the cathode compositions. J. Electrochem. Soc. *123*, 1262–1264.

6. Whittingham, M.S. (1978). Chemistry of intercalation compounds: metal guests in chalcogenide hosts. Prog. Solid State Chem. *12*, 41–99.

7. Whittingham, M.S. (1976). Electrical energy storage and intercalation chemistry. Science *192*, 1126–1127.

8. Winter, M., Barnett, B., and Xu, K. (2018). Before Li ion batteries. Chem. Rev. *118*, 11433–11456.

9. Nakajima, K. (1989). Conversation too hot to handle. Mainichi Daily News, 1.

10. Mizushima, K., Jones, P.C., Wiseman, P.J., and Goodenough, J.B. (1980). Li_xCoO_2 ($0<x\leq1$): a new cathode material for batteries of high energy density. Mater. Res. Bull. *15*, 783–789.

11. Thackeray, M.M., Johnson, P.J., De Picciotto, L.A., Bruce, P.G., and Goodenough, J.B. (1984). Electrochemical extraction of lithium from $LiMn_2O_4$. Mater. Res. Bull. *19*, 179–187.

12. Guyomard, D., and Tarascon, J. (1993). Rechargeable $Li_{1+x}Mn_2O_4$/carbon cells with a new electrolyte composition potentiostatic studies and application to practical cells. J. Electrochem. Soc. *140*, 3071–3081.

13. Yazami, R., and Touzain, P. (1983). A reversible graphite-lithium negative electrode for electrochemical generators. J. Power Sources *9*, 365–371.

14. Rossouw, M.H., Liles, D.C., and Thackeray, M.M. (1993). Synthesis and structural characterization of a novel layered lithium manganese oxide, $Li_{0.36}Mn_{0.91}O_2$, and its lithiated derivative, $Li_{1.09}Mn_{0.91}O_2$. J. Solid State Chem. *104*, 464–466.

15. Johnson, C.S., Kim, J., Lefief, C., Li, N., Vaughey, J.T., and Thackeray, M.M. (2004). The significance of the Li_2MnO_3 component in 'composite' xLi2MnO3·(1−x) LiMn0.5Ni0.5O2 electrodes. Electrochem. Commun. *6*, 1085–1091.

16. Padhi, A.K., Nanjundaswamy, K.S., and Goodenough, J.B. (1997). Phospho-olivines as positive-electrode materials for rechargeable lithium batteries. J. Electrochem. Soc. *144*, 1188–1194.

17. Numata, K., Sakaki, C., and Yamanaka, S. (1997). Synthesis of solid solutions in a system of $LiCoO_2$-Li_2MnO_3 for cathode materials of secondary lithium batteries. Chem. Lett. *26*, 725–726.

18. Mustarelli, P., Massarotti, V., Bini, M., and Capsoni, D. (1997). Transferred hyperfine interaction and structure in $LiMn_2O_4$ and Li_2MnO_3 coexisting phases: mA XRD and Li 7 NMR-MAS study. Phys. Rev. B *55*, 12018–12024.

19. Kim, J.S., Johnson, C.S., and Thackeray, M.M. (2002). Layered $xLiMO_2\cdot(1\text{-}x)Li_2M'O_3$ electrodes for lithium batteries: a study of $0.95LiMn_{0.5}Ni_{0.5}O_2\cdot0.05Li_2TiO_3$. Electrochem. Commun. *4*, 205–209.

20. Yabuuchi, N., and Ohzuku, T. (2003). Novel lithium insertion material of $LiCo_{1/3}Ni_{1/3}Mn_{1/3}O_2$ for advanced lithium-ion batteries. J. Power Sources *119–121*, 171–174.

21. Belharouak, I., Sun, Y.-K., Liu, J., and Amine, K. (2003). $Li(Ni_{1/3}Co_{1/3}Mn_{1/3})O_2$ as a suitable cathode for high power applications. J. Power Sources *123*, 247–252.

22. Li, H., Huang, X.J., and Chen, L.Q. (1997) One type rechargeable lithium battery. China Patent, ZL97112460.4.

23. Ohzuku, T., Ueda, A., and Yamamoto, N. (1995). Zero-strain insertion material of Li $[Li_{1/3}Ti_{5/3}]O_4$ for rechargeable lithium cells. J. Electrochem. Soc. *142*, 1431–1435.

24. Yang, J., Takeda, Y., Imanishi, N., Capiglia, C., Xie, J.Y., and Yamamoto, O. (2002). SiO_x-based anodes for secondary lithium batteries. Solid State Ionics *152–153*, 125–129.

25. Lin, D., Liu, Y., and Cui, Y. (2017). Reviving the lithium metal anode for high-energy batteries. Nat. Nanotechnol. *12*, 194–206.

26. Cheng, X.B., Zhang, R., Zhao, C.Z., and Zhang, Q. (2017). Toward safe lithium metal anode in rechargeable batteries: a review. Chem. Rev. *117*, 10403–10473.

27. Wang, L., Wang, Q., Jia, W., Chen, S., Gao, P., and Li, J. (2017). Li metal coated with amorphous Li_3PO_4 via magnetron sputtering for stable and long-cycle life lithium metal batteries. J. Power Sources *342*, 175–182.

28. Qian, J., Henderson, W.A., Xu, W., Bhattacharya, P., Engelhard, M., Borodin, O., and Zhang, J.G. (2015). High rate and stable cycling of lithium metal anode. Nat. Commun. *6*, 6362.

29. Liu, Y., and Cui, Y. (2017). Lithium metal anodes: a recipe for protection. Joule *1*, 649–650.

30. Zhang, Z., Shao, Y., Lotsch, B., Hu, Y., Li, H., Janek, J., Nazar, L.F., Nan, C., Maier, J., Armand, M., et al. (2018). New horizons for inorganic solid state ion conductors. Energy Environ. Sci. *11*, 1945–1976.

31. Manthiram, A., Yu, X., and Wang, S. (2017). Lithium battery chemistries enabled by solid-state electrolytes. Nat. Rev. Mater. *2*, 16103.

32. Kato, Y., Hori, S., Saito, T., Suzuki, K., Hirayama, M., Mitsui, A., Yonemura, M., Iba, H., and Kanno, R. (2016). High-power all-solid-state batteries using sulfide superionic conductors. Nat. Energy *1*, 16030.

33. Nolan, A.M., Zhu, Y., He, X., Bai, Q., and Mo, Y. (2018). Computation-accelerated design of materials and interfaces for all-solid-state lithium-ion batteries. Joule *2*, 1–4.

34. Hovington, P., Lagacé, M., Guerfi, A., Bouchard, P., Mauger, A., Julien, C.M., Armand, M., and Zaghib, K. (2015). New lithium metal polymer solid state battery for an ultrahigh energy: Nano C-$LiFePO_4$ versus nano $Li_{1.2}V_3O_8$. Nano Lett. *15*, 2671–2678.

35. Eshetu, G.G., Armand, M., and Passerini, S. (2018). Lithium Polymer Electrolytes and Batteries. Series on Chemistry, Energy and the Environment (World Scientific), pp. 319–364.

36. Poizot, P., Laruelle, S., Grugeon, S., Dupont, L., and Tarascon, J.M. (2000). Nano-sized transition-metal oxides as negative-electrode materials for lithium-ion batteries. Nature *407*, 496–499.

37. Zu, C.X., and Li, H. (2011). Thermodynamic analysis on energy densities of batteries. Energy Environ. Sci. *4*, 2614–2624.

38. Wu, F.X., and Yushin, G. (2017). Conversion cathodes for rechargeable lithium and lithium-ion batteries. Energy Environ. Sci. *10*, 435–459.

39. Arai, H., Okada, S., Sakurai, Y., and Yamaki, J. (1997). Cathode performance and voltage estimation of metal trihalides. J. Power Sources *68*, 716–719.

40. Hua, X., Robert, R., Du, L.S., Wiaderek, K.M., Leskes, M., Chapman, K.W., Chupas, P.J., and Grey, C.P. (2014). Comprehensive study of the CuF_2 conversion reaction mechanism in a lithium ion battery. J. Phys. Chem. C *118*, 15169–15184.

41. Wang, F., Yu, H.C., Chen, M.H., Wu, L., Pereira, N., Thornton, K., Van der Ven, A., Zhu, Y., Amatucci, G.G., and Graetz, J. (2012). Tracking lithium transport and electrochemical reactions in nanoparticles. Nat. Commun *3*, 1201.

42. Amatucci, G.G., and Pereira, N. (2007). Fluoride based electrode materials for advanced energy storage devices. J. Fluor. Chem. *128*, 243–262.

43. Boebinger, M.G., Yeh, D., Xu, M., Miles, B.C., Wang, B., Papakyriakou, M., Lewis, J.A., Kondekar, N.P., Cortes, F.J.Q., and Hwang, S. (2018). Avoiding fracture in a conversion battery material through reaction with larger ions. Joule *2*, 1–4.

44. Barin, I., and Platzki, G. (1995). Thermochemical Data of Pure Compounds, Third edition (VCH Publishers).

45. Doe, R.E., Persson, K.A., Meng, Y.S., and Ceder, G. (2008). First-principles investigation of the Li-Fe-F phase diagram and equilibrium and nonequilibrium conversion reactions of iron fluorides with lithium. Chem. Mater. *20*, 5274–5283.

46. Ko, J.K., Wiaderek, K.M., Pereira, N., Kinnibrugh, T.L., Kim, J.R., Chupas, P.J., Chapman, K.W., and Amatucci, G.G. (2014). Transport, phase reactions, and hysteresis of iron fluoride and oxyfluoride conversion electrode materials for lithium batteries. ACS Appl. Mater. Inter. *6*, 10858–10869.

47. Yu, S.H., Feng, X.R., Zhang, N., Seok, J., and Abruña, H.D. (2018). Understanding conversion-type electrodes for lithium rechargeable batteries. Acc. Chem. Res. *51*, 273–281.

48. Manthiram, A., Chung, S.H., and Zu, C.X. (2015). Lithium-sulfur batteries: progress and prospects. Adv. Mater *27*, 1980–2006.

49. Lv, D.P., Zheng, J.M., Li, Q.Y., Xie, X., Ferrara, S., Nie, Z.M., Mehdi, L.B., Browning, N.D., Zhang, J.G., Graff, G.L., et al. (2015). High energy density lithium-sulfur batteries: challenges of thick sulfur cathodes. Adv. Energy Mater. *5*.

50. Lam, P., and Yazami, R. (2006). Physical characteristics and rate performance of (CFx)n (0.33< x< 0.66) in lithium batteries. J. Power Sources *153*, 354–359.

51. Reddy, M.A., Breitung, B., and Fichtner, M. (2013). Improving the energy density and power density of CF_x by mechanical milling: a primary lithium battery electrode. ACS Appl. Mater. Inter. *5*, 11207–11211.

52. Lascaud, M., Lachter, A., Salardenne, J., and Barrière, A.S. (1979). Electrical conduction mechanisms in FeF_3 thin films. Thin Solid Films *59*, 353–360.

53. Fu, W.B., Zhao, E.B., Sun, Z.F., Ren, X.L., Magasinski, A., and Yushin, G. (2018). Iron fluoride-carbon nanocomposite nanofibers as free-standing cathodes for high-energy lithium batteries. Adv. Funct. Mater. *28*.

54. Groult, H., Neveu, S., Leclerc, S., Porras-Gutierrez, A.-G., Julien, C.M., Tressaud, A., Durand, E., Penin, N., and Labrugere, C. (2017). Nano-CoF_3 prepared by direct fluorination with F_2 gas: application as electrode material in Li-ion battery. J. Fluor. Chem. *196*, 117–127.

55. Wang, D.Y., Gong, M., Chou, H.L., Pan, C.J., Chen, H.A., Wu, Y.P., Lin, M.C., Guan, M.Y., Yang, J., Chen, C.W., et al. (2015). Highly active and stable hybrid catalyst of cobalt-doped FeS_2 nanosheets-carbon nanotubes for hydrogen evolution reaction. J. Am. Chem. Soc. *137*, 1587–1592.

56. Xu, X., Cai, T.W., Meng, Z., Ying, H.J., Xie, Y., Zhu, X.L., and Han, W.Q. (2016). FeS_2 nanocrystals prepared in hierarchical porous carbon for lithium-ion battery. J. Power Sources *331*, 366–372.

57. Tang, W.P., Yang, X.J., Liu, Z.H., and Ooi, K. (2003). Preparation of beta-MnO_2 nanocrystal/acetylene black composites for lithium batteries. J. Mater. Chem. *13*, 2989–2995.

58. Zang, J., Ye, J.C., Qian, H., Lin, Y., Zhang, X.W., Zheng, M.S., and Dong, Q.F. (2018). Hollow carbon sphere with open pore encapsulated MnO_2 nanosheets as high-performance anode materials for lithium ion batteries. Electrochim. Acta *260*, 783–788.

59. Krahl, T., Winkelmann, F.M., Martin, A., Pinna, N., and Kemnitz, E. (2018). Novel synthesis of anhydrous and hydroxylated CuF_2 nanoparticles and their potential for lithium ion batteries. Chem. Eur. J. *24*, 7177–7187.

60. Balaya, P., and Maier, J. (2010). Thermodynamics of nano-and macrocrystalline anatase using cell voltage measurements. Phys. Chem. Chem. Phys. *12*, 215–219.

61. Li, H., Balaya, P., and Maier, J. (2004). Li-storage via heterogeneous reaction in selected binary metal fluorides and oxides. J. Electrochem. Soc. *151*, A1878–A1885.

62. Balaya, P., Bhattacharyya, A.J., Jamnik, J., Zhukovskii, Y.F., Kotomin, E.A., and Maier, J. (2006). Nano-ionics in the context of lithium batteries. J. Power Sources *159*, 171–178.

63. Seo, J.K., Cho, H., Takahara, K., Chapman, K.W., Borkiewicz, O.J., Sina, M., and Shirley Meng, Y. (2017). Revisiting the conversion reaction voltage and the reversibility of the CuF_2 electrode in Li-ion batteries. Nano Res. *10*, 4232–4244.

64. Yersak, T.A., Macpherson, H.A., Kim, S.C., Le, V., Kang, C.S., Son, S.B., Kim, Y.H., Trevey, J.E., Oh, K.H., Stoldt, C., et al. (2013). Solid state enabled reversible four electron storage. Adv. Energy Mater. *3*, 120–127.

65. Chen, S.L., Wang, L.P., Shao, R.W., Zou, J., Cai, R., Lin, J.H., Zhu, C.Y., Zhang, J.M., Xu, F., Cao, J., et al. (2018). Atomic structure and migration dynamics of MoS_2/Li_xMoS_2 interface. Nano Energy *48*, 560–568.

66. Karki, K., Wu, L., Ma, Y., Armstrong, M.J., Holmes, J.D., Garofalini, S.H., Zhu, Y., Stach, E.A., and Wang, F. (2018). Revisiting conversion reaction mechanisms in lithium batteries: lithiation-driven topotactic transformation in FeF_2. J. Am. Chem. Soc. *140*, 17915–17922.

67. Sina, M., Nam, K.-W., Su, D., Pereira, N., Yang, X.-Q., Amatucci, G.G., and Cosandey, F. (2013). Structural phase transformation and Fe valence evolution in FeO_xF_{2-x}/C nanocomposite electrodes during lithiation and de-lithiation processes. J. Mater. Chem. A *1*, 11629–11640.

68. Thackeray, M.M. (1997). Manganese oxides for lithium batteries. Prog. Solid State Chem. *25*, 1–71.

69. Li, L., Jacobs, R., Gao, P., Gan, L., Wang, F., Morgan, D., and Jin, S. (2016). Origins of large voltage hysteresis in high-energy-density metal fluoride lithium-ion battery conversion electrodes. J. Am. Chem. Soc. *138*, 2838–2848.

70. Sauvage, F., Tarascon, J.-M., and Baudrin, E. (2007). In situ measurements of Li ion battery electrode material conductivity: application to Li_xCoO_2 and conversion reactions. J. Phys. Chem. C *111*, 9624–9630.

71. Wang, F., Robert, R., Chernova, N.A., Pereira, N., Omenya, F., Badway, F., Hua, X., Ruotolo, M., Zhang, R., Wu, L., et al. (2011). Conversion reaction mechanisms in lithium ion batteries: study of the binary metal fluoride electrodes. J. Am. Chem. Soc. *133*, 18828–18836.

72. Balaya, P., Li, H., Kienle, L., and Maier, J. (2003). Fully reversible homogeneous and heterogeneous Li storage in RuO_2 with high capacity. Adv. Funct. Mater. *13*, 621–625.

73. Wang, L.P., Li, H., Huang, X.J., and Baudrin, E. (2011). A comparative study of Fd-3m and P4(3)32. Solid State Ionics *193*, 32–38.

74. Hwang, B.J., Tsai, Y.W., Carlier, D., and Ceder, G. (2003). A combined computational/experimental study on $LiNi_{1/3}Co_{1/3}Mn_{1/3}O_2$. Chem. Mater. *15*, 3676–3682.

75. Zhao, J., Zou, X.X., Zhu, Y.J., Xu, Y.H., and Wang, C.S. (2016). Electrochemical intercalation of potassium into graphite. Adv. Funct. Mater. *26*, 8103–8110.

76. Betz, J., Bieker, G., Meister, P., Placke, T., Winter, M., and Schmuch, R. (2018). Theoretical versus practical energy: a plea for more transparency in the energy calculation of different rechargeable battery systems. Adv. Energy Mater.

77. Lin, Z., Liu, T., Ai, X., and Liang, C. (2018). Aligning academia and industry for unified battery performance metrics. Nat. Commun *9*, 5262.

78. Thieu, D.T., Fawey, M.H., Bhatia, H., Diemant, T., Chakravadhanula, V.S.K., Behm, R.J., Kübel, C., and Fichtner, M. (2017). CuF_2 as reversible cathode for fluoride ion batteries. Adv. Funct. Mater. *27*.

79. Rosenman, A., Markevich, E., Salitra, G., Aurbach, D., Garsuch, A., and Chesneau, F.F. (2015). Review on Li-sulfur battery systems: an integral perspective. Adv. Energy Mater. *5*.

80. Pereira, N., Badway, F., Wartelsky, M., Gunn, S., and Amatucci, G.G. (2009). Iron oxyfluorides as high capacity cathode materials for lithium batteries. J. Electrochem. Soc. *156*, A407–A416.

81. Gao, P., Zhang, Y.-Y., Wang, L., Chen, S., Huang, Y., Ma, X., Liu, K., and Yu, D. (2017). In situ atomic-scale observation of reversible sodium ions migration in layered metal dichalcogenide SnS_2 nanostructures. Nano Energy *32*, 302–309.

82. Bruce, P.G., Scrosati, B., and Tarascon, J.M. (2008). Nanomaterials for rechargeable lithium batteries. Angew. Chem. Int. Ed. Engl. *47*, 2930–2946.

83. Badway, F., Mansour, A.N., Pereira, N., Al-Sharab, J.F., Cosandey, F., Plitz, I., and Amatucci, G.G. (2007). Structure and electrochemistry of copper fluoride nanocomposites utilizing mixed conducting matrices. Chem. Mater. *19*, 4129–4141.

84. Badway, F., Pereira, N., Cosandey, F., and Amatucci, G.G. (2003). Carbon-metal fluoride nanocomposites-structure and electrochemistry of FeF_3:C. J. Electrochem. Soc. *150*, A1209–A1218.

85. Titirici, M.M., White, R.J., Brun, N., Budarin, V.L., Su, D.S., del Monte, F., Clark, J.H., and MacLachlan, M.J. (2015). Sustainable carbon materials. Chem. Soc. Rev. *44*, 250–290.

86. Gu, W., Magasinski, A., Zdyrko, B., and Yushin, G. (2015). Metal fluorides nanoconfined in carbon nanopores as reversible high capacity cathodes for Li and Li-ion rechargeable batteries: FeF_2 as an example. Adv. Energy Mater. *5*.

87. Liu, J., Wen, Y.R., Wang, Y., van Aken, P.A., Maier, J., and Yu, Y. (2014). Carbon-encapsulated pyrite as stable and earth-abundant high energy cathode material for rechargeable lithium batteries. Adv. Mater. *26*, 6025–6030.

88. Son, S.B., Yersak, T.A., Piper, D.M., Kim, S.C., Kang, C.S., Cho, J.S., Suh, S.S., Kim, Y.U., Oh, K.H., and Lee, S.H. (2014). A stabilized PAN-FeS_2 cathode with an EC/DEC liquid electrolyte. Adv. Energy Mater. *4*.

89. Dong, Y.F., Liu, S.H., Wang, Z.Y., Liu, Y., Zhao, Z.B., and Qiu, J.S. (2015). Sulfur-infiltrated graphene-backboned mesoporous carbon nanosheets with a conductive polymer coating for long-life lithium-sulfur batteries. Nanoscale *7*, 7569–7573.

90. Ma, D.L., Cao, Z.Y., Wang, H.G., Huang, X.L., Wang, L.M., and Zhang, X.B. (2012). Three-dimensionally ordered macroporous FeF_3 and its in situ homogenous polymerization coating for high energy and power density lithium ion batteries. Energy Environ. Sci. *5*, 8538–8542.

91. Wang, F., Kim, S.W., Seo, D.H., Kang, K., Wang, L.P., Su, D., Vajo, J.J., Wang, J., and Graetz, J. (2015). Ternary metal fluorides as high-energy cathodes with low cycling hysteresis. Nat. Commun. *6*, 6668.

92. Fan, X.L., Hu, E.Y., Ji, X., Zhu, Y.Z., Han, F.D., Hwang, S.Y., Liu, J., Bak, S.M., Ma, Z.H., Gao, T., et al. (2018). High energy-density and reversibility of iron fluoride cathode enabled via an intercalation-extrusion reaction. Nat. Commun. *9*, 2324.

93. Wei, Z.X., Wang, D.X., Yang, X., Wang, C.Z., Chen, G., and Du, F. (2018). From crystalline to amorphous: an effective avenue to engineer high-performance electrode materials for sodium-ion batteries. Adv. Mater. Interfaces *5*.

94. Cui, Y.-H., Xue, M.-Z., Zhou, Y.-N., Peng, S.-M., Wang, X.-L., and Fu, Z.-W. (2011). The investigation on electrochemical reaction mechanism of CuF_2 thin film with lithium. Electrochim. Acta *56*, 2328–2335.

95. Lee, J.M., Hwang, H.S., Cho, W.I., Cho, B.W., and Kim, K.Y. (2004). Effect of silver co-sputtering on amorphous V_2O_5 thin-films for microbatteries. J. Power Sources *136*, 122–131.

96. Liu, W., Li, Y., Zhan, B.-X., Shi, B., Guo, R., Pei, H.-J., Xie, J.-Y., and Fu, Z.-W. (2016). Amorphous, highly disordered carbon fluorides as a novel cathode for sodium secondary batteries. J. Phys. Chem. C *120*, 25203–25209.

97. Zhang, T.B., Cheng, X.B., Zhang, Q., Lu, Y.C., and Luo, G.S. (2016). Construction of a cathode using amorphous $FePO_4$ nanoparticles for a high-power/energy-density lithium-ion battery with long-term stability. J. Power Sources *324*, 52–60.

98. Uchaker, E., Zheng, Y.Z., Li, S., Candelaria, S.L., Hu, S., and Cao, G.Z. (2014). Better than crystalline: amorphous vanadium oxide for sodium-ion batteries. J. Mater. Chem. A *2*, 18208–18214.

99. Delmer, O., Balaya, P., Kienle, L., and Maier, J. (2008). Enhanced potential of amorphous electrode materials: case study of RuO_2. Adv. Mater. *20*, 501–505.

100. Song, Y.N., Yang, S.F., Zavalij, P.Y., and Whittingham, M.S. (2002). Temperature-dependent properties of $FePO_4$ cathode materials. Mater. Res. Bull. *37*, 1249–1257.

101. Yu, L., Wang, H.-X., Liu, Z.-Y., and Fu, Z.-W. (2010). Pulsed laser deposited FeOF as negative electrodes for rechargeable Li batteries. Electrochim. Acta *56*, 767–775.

102. Zhang, H., Zhou, Y.-N., Sun, Q., and Fu, Z.-W. (2008). Nanostructured nickel fluoride thin film as a new Li storage material. Solid State Sci. *10*, 1166–1172.

103. Yuan, Y., Liu, C., Byles, B.W., Yao, W., Song, B., Cheng, M., Huang, Z., Amine, K., Pomerantseva, E., and Shahbazian-Yassar, R. (2018). Ordering heterogeneity of $[MnO_6]$ octahedra in tunnel-structured MnO_2 and its influence on ion storage. Joule *3*, 1–14.

104. Kitchaev, D.A., Peng, H.W., Liu, Y., Sun, J.W., Perdew, J.P., and Ceder, G. (2016). Energetics of MnO_2 polymorphs in density functional theory. Phys. Rev. B *93*.

105. Jiao, F., and Bruce, P.G. (2007). Mesoporous crystalline β-MnO_2—a reversible positive electrode for rechargeable lithium batteries. Adv. Mater. *19*, 657–660.

106. Masset, P.J., and Guidotti, R.A. (2008). Thermal activated ("thermal") battery technology - Part IIIa: FeS_2 cathode material. J. Power Sources *177*, 595–609.

107. Tomm, Y., Schieck, R., Ellmer, K., and Fiechter, S. (1995). Growth-mechanism and electronic-properties of doped pyrite Fes_2 crystals. J. Cryst. Growth *146*, 271–276.

108. Badway, F., Cosandey, F., Pereira, N., and Amatucci, G.G. (2003). Carbon metal fluoride nanocomposites-high-capacity reversible metal fluoride conversion materials as rechargeable positive electrodes for Li batteries. J. Electrochem. Soc. *150*, A1318–A1327.

109. Gu, W.T., Borodin, O., Zdyrko, B., Lin, H.T., Kim, H., Nitta, N., Huang, J.X., Magasinski, A., Milicev, Z., Berdichevsky, G., et al. (2016). Lithium-iron fluoride battery with in situ surface protection. Adv. Funct. Mater. *26*, 1507–1516.

110. Zhao, E.B., Borodin, O., Gao, X.S., Lei, D.N., Xiao, Y.R., Ren, X.L., Fu, W.B., Magasinski, A., Turcheniuk, K., and Yushin, G. (2018). Lithium-iron (III) fluoride battery with double surface protection. Adv. Energy Mater. *8*.

111. Strauss, E., Golodnitsky, D., and Peled, E. (2000). Study of phase changes during 500 full cycles of Li/composite polymer electrolyte/FeS_2 battery. Electrochim. Acta *45*, 1519–1525.

112. Luo, J.Y., Zhang, J.J., and Xia, Y.Y. (2006). Highly electrochemical reaction of lithium in the ordered mesoporosus beta-MnO_2. Chem. Mater. *18*, 5618–5623.

113. Wang, L., Zou, J., Chen, S., Zhou, G., Bai, J., Gao, P., Wang, Y., Yu, X., Li, J., Hu, Y.-S., et al. (2018). TiS_2 as a high performance potassium ion battery cathode in ether-based electrolyte. Energy Storage Mater. *12*, 216–222.

114. Luo, F., Liu, B., Zheng, J., Chu, G., Zhong, K., Li, H., Huang, X., and Chen, L. (2015). Review—Nano-silicon/carbon composite anode materials towards practical application for next generation Li-ion batteries. J. Electrochem. Soc. *162*, A2509–A2528.

115. Choi, J.W., and Aurbach, D. (2016). Promise and reality of post-lithium-ion batteries with high energy densities. Nat. Rev. Mater. *1*, 16013.

116. Luo, F., Chu, G., Xia, X., Liu, B., Zheng, J., Li, J., Li, H., Gu, C., and Chen, L. (2015). Thick solid electrolyte interphases grown on silicon nanocone anodes during slow cycling and their negative effects on the performance of Li-ion batteries. Nanoscale *7*, 7651–7658.